# Low-Frequency Characterization of MEMS-based Portable Atomic Magnetometer

Rahul R. Mhaskar*†, Svenja Knappe*† and John Kitching*
*Time and Frequency Division, National Institute for Standards and Technology, Boulder, CO 80305
†University of Colorado, Boulder, CO 80309
Email: Rahul.Mhaskar@nist.gov

*Abstract*— Atomic magnetometers based on absorption or polarization rotation of light in an alkali vapor have recently demonstrated sensitivities rivaling those of superconducting quantum interference devices (SQUIDs) [1]. Miniaturization of such devices containing vapor cells fabricated with micro–electro–mechanical (MEMS) technology has been the focus of development for the better part of the last decade. In this paper, we describe a portable magnetometry system with a sensitivity below 50 fT/$\sqrt{\text{Hz}}$ at 100 Hz. The atomic magnetometer consists of a microfabricated sensor head that is fiber coupled to a control module consisting of a laser and electronics. We describe the construction of this system and present the results of sensitivity measurements with an emphasis on identifying and characterizing the source of *1/f* (flicker) noise. This portable magnetometer system was developed to measure magnetocardiograms (MCG) of human subjects inside a shielded environment [2].

## I. INTRODUCTION

The field of high-sensitivity magnetometry is dominated by SQUIDs, which are used commercially in numerous applications where sub-100 fT/$\sqrt{\text{Hz}}$ sensitivity at low frequencies (0.01–100 Hz) is essential. This technology has led to significant advances in diverse fields such as medicine, geology, national security and oil exploration [3]. Biomedical applications benefiting from this technology include magnetocardiography (MCG) and magnetoencephalography (MEG), where the signal strengths are typically in the range 1–100 pT for the former and below 1 pT in the latter case [4]. Cryogenic operation, however, makes the use of SQUID magnetometers for these applications cumbersome and expensive, and it often requires specialized personnel to operate them. In order to make highly sensitive magnetometers more accessible for a wide range of applications, they need not only have high sensitivity at low frequencies, but they should also be inexpensive, portable, easy to operate without cryogenics, and operate in a magnetically unshielded environment.

Atomic magnetometers, based on absorption or polarization rotation of light in alkali vapors, have achieved sensitivities similar to SQUIDs in the past decade [1]. The technological development of miniaturized alkali vapor cells for use in Chip-Scale Atomic Clocks (CSACs) [5], can be leveraged to miniaturize atomic magnetometers, as demonstrated in ref. [6]. The advantage of such Chip-Scale Atomic Magnetometers (CSAMs) is that the sensors can be very small, of the order 1 cm, and can therefore be placed a few millimeters from the source. Because many of the magnetic signals of biological

origin scale as $1/r^3$ where $r$ is the distance between the source and the sensor [3], the improvement in the signal-to-noise ratio (SNR) can be significant. In addition, CSAMs can be fiber coupled and operated remotely [7], do not need to be cryogenically cooled, and have low power consumption. They are fabricated by use of well-established optical MEMS technology [8], and could be mass-produced in large quantities. All these factors contribute toward making these devices inexpensive and easy to operate. In this paper, we characterize the performance of a portable magnetometry system at low frequencies (0.1–10 Hz).

## II. PHYSICS

Atomic magnetometers are based on the fact that the collective spin polarization of atoms precesses in the presence of a magnetic field (Larmor precession), which can then be optically interrogated [9]. Typically, alkali atoms are used in part because of their simple atomic structure. One interrogation method uses resonant magnetic field oscillating at the frequency of Larmor precession. The precessing atomic polarization can be detected as a modulation on light illuminating the vapor [10]. Another method relies on absorption of light in an atomic vapor. The vapor is spin-polarized with circularly polarized light resonant with an atomic transition. When detecting absorption, the atomic polarization reduces the absorption of light on the D1 line in the absence of a magnetic field. In presence of a magnetic field, the atoms precess about the field and the absorption of light increases. Thus, a resonance peak centered around zero magnetic field can be observed in the light transmitted through the atomic vapor and can be used to measure the magnetic field [11], [12]. When the magnetometer is operated at high alkali atom density, where the inter-atomic spin-exchange collision rate is much higher than the Larmor precession frequency, the magnetometer can operate in the so-called Spin-Exchange Relaxation-Free (SERF) regime [13]. Here, the broadening of the resonance line through spin-exchange collisions is suppressed, which allows for high signal-to-noise ratio while still maintaining narrow resonance line-width.

## III. MAGNETOMETER SETUP

The portable atomic magnetometry system consists of a CSAM sensor head, a distributed feedback (DFB) laser at 795 nm and control electronics. The light is delivered to the
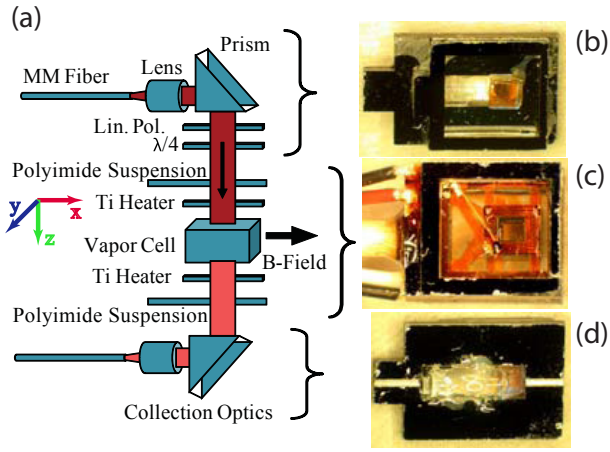
Fig. 1. (a) A schematic of the sensor head. (b) The light collimator and polarizer layer, bottom view. (c) The light collection and out-coupling layer. The prism, GRIN lens and the groove for the fiber are visible. (d) The vapor cell suspension layer. The spiral Ti traces can be seen beneath the orange polyimide suspension.

sensor head through a multimode fiber. The sensor head has a volume of 0.75 cm$^3$ and the center of the vapor cell can be placed as close as $\sim$2.5 mm from the the surface of the sample.

### A. Sensor–head Fabrication

The sensor–head is fabricated using three layers: one for collimation of the optical fiber output (Fig. 1(b)), one containing the vapor cell (Fig. 1(d)), and the third for coupling the transmitted light into the output optical fiber (Fig. 1(c)). Features, such as slots to place micro-optic components, are etched into 1 mm thick silicon wafers. The output of the incoming fiber is collimated using a GRIN lens to produce a collimated light beam of $\sim$1 mm diameter. The light is reflected at right angle by a prism and circularly polarized with a film polarizer and a quarter-wave retarder. The light then passes through the cell and is reflected by a second right-angle prism onto another GRIN lens that focuses it onto the outgoing optical fiber.

The vapor cell has an internal volume of (2 mm)$^3$ and external dimensions of 3mm×3mm×2.6mm. The cell contains metallic $^{87}$Rb and nitrogen buffer gas with number density of $\sim 4.5 \times 10^{25}$ m$^{-3}$. The vapor cell fabrication procedure is described in ref. [14]. Two heaters are glued to the top and bottom windows of the cell. The assembly is suspended in a silicon frame using laser-cut polyimide tethers to thermally isolate the cell from the silicon housing. Electrical connections to the heaters are provided by gold traces deposited over a glass bridge supported on the suspension. The gold traces are wire-bonded to gold pads on the heaters and on the frame. Wires are glued to the gold pads on the frame using conductive epoxy.

The cell heaters are fabricated on a pyrex substrate 300 $\mu$m thick. Two spiral titanium patterns with 200 $\mu$m wide traces are evaporated onto the substrate, separated by a 2 $\mu$m thick
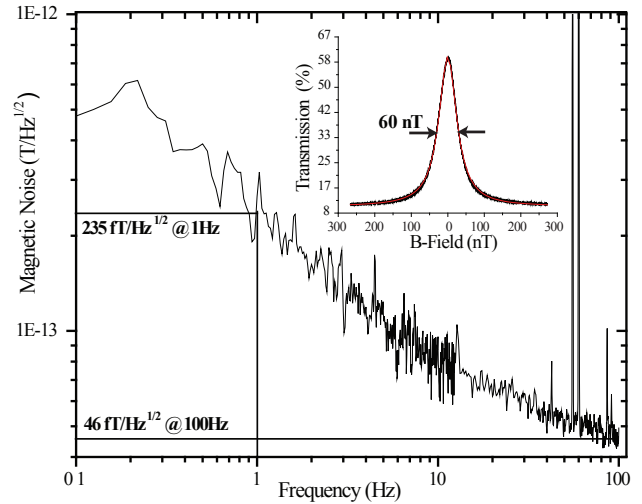


Fig. 2. The main figure shows the magnetic-field-referred noise measured for the CSAM as a function of frequency. Subsequent measurements have shown that the response curve flattens above 100 Hz. Inset: The transmission curve for light through the alkali vapor as a function of magnetic field.

SU-8 passivation layer. The two Ti layers are connected in series such that current flows in opposite directions in adjacent traces both in- and out-of-plane of the substrate. This design was chosen to minimize the magnetic fields produced by the current flowing through the heater traces. The resistance of one such heater is $\sim$ 200 $\Omega$.

### IV. DEVICE PERFORMANCE CHARACTERIZATION

The CSAM was characterized in a magnetically shielded environment consisting of three $\mu$-metal shields. The vapor cell was heated to $\sim$ 160 °C by continuously driving the heaters with a sinusoidal voltage at 30 kHz. The power dissipation in the heaters was $\sim$ 350 mW. The vapor cell was illuminated with $\sim$ 300 $\mu$W optical power and the transmitted light collected by the optical fiber was detected on a photodiode. When the magnetic field was scanned around zero, the light transmission spectrum showed close to a Lorentzian line-shape with a full width at half maximum (FWHM) of 60 nT and a contrast between the baseline absorption and resonance peak of $\sim$50 %, as shown in the inset of Fig. 2. An additional B-field in the direction of the measured B-field, modulated at $\sim$1.1 kHz, allowed the use of phase-sensitive detection yielding a dispersive line-shape [15]. The magnetometer response to changes in the magnetic field projection in the direction of the modulation field was calibrated using the slope of the dispersive curve at the zero-crossing. The applied B-field was zeroed and the signal was analyzed using a fast fourier transform (FFT) to determine the sensitivity of the device as the noise equivalent magnetic field. This sensitivity is shown in Fig. 2.

We obtained a sensitivity of $\sim$ 50 fT$_{\mathrm{rms}}/\sqrt{\mathrm{Hz}}$ at 100 Hz increasing to $\sim$ 250 fT$_{\mathrm{rms}}/\sqrt{\mathrm{Hz}}$ at 1 Hz. The bandwidth of the magnetometer was measured to be 250 Hz, by measuring the response of the magnetometer to a calibrated oscillating
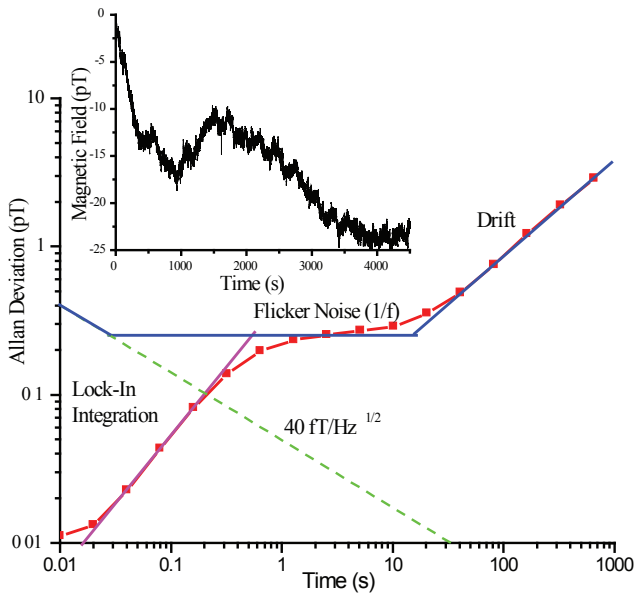
Fig. 3. This figure shows the Allan deviation of the CSAM output attributed to white noise (green) and lock-in amplifier integration time constant (magenta). The projected stability of the CSAM output is indicated by the blue curve. The red curve shows the Allan deviation calculated for the long term data shown in the inset. Inset: output of the CSAM over a period of 1.5 hours.

magnetic field. The sensitivity is constant beyond 100 Hz and deteriorates above 150 Hz due to bandwidth limitations. We modeled the magnetic noise produced by thermal currents in the Ti heater traces using the method described in ref. [16]. We found that the heaters produce a white noise of $\sim 35~\mathrm{fT_{rms}}/\sqrt{\mathrm{Hz}}$ at the center of the cell. Thus, we believe that beyond 100 Hz we are limited by the magnetic noise produced by our heaters.

## V. INVESTIGATION OF LOW FREQUENCY NOISE

From the sensitivity measurement, we find that below about 100 Hz, the magnetic-field-referred noise is dominated by $1/f$ or the so-called flicker noise. The most likely flicker noise sources are sudden changes in the material properties of the heater [17] and the heater drive current. To characterize the low frequency behavior of the CSAM, we monitored the sensor output over a few hours, as shown in inset of Fig. 3. We find that the sensor output drifts by tens of picoTeslas over the measurement period. Calculating the Allan deviation represented by the red curve in Fig. 3, we find that the drift dominates beyond a measurement period of approximately 15 s. The drift in CSAM output is qualitatively similar to that observed in the rms current through the heaters. This drift can be attributed to slowly varying parameters such as the vapor cell temperature due to the changing heater drive current and ambient temperature.

To test the hypothesis that the drift arises from heater current changes, we quantified the magnetometer response to change in the rms current through the heaters by modulating the amplitude of the heater drive current at different frequencies
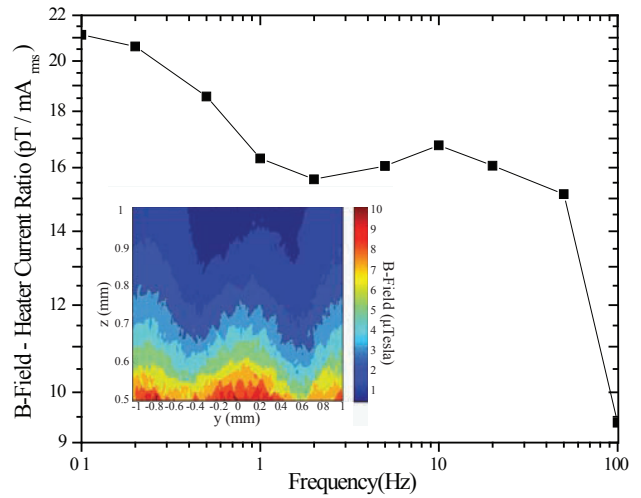


Fig. 4. This figure shows the change in magnetometer output per $\mathrm{mA_{rms}}$ change in the magnitude of the AC heater current, as a function of the frequency of AM applied to the heater drive. The response at 100 Hz is diminished due to lock-in amplifier bandwidth. The inset shows the calculated magnetic field due to 50 mA current through the heater. The vapor cell extends in the z-direction from 0.3 mm to 2.3 mm.

and observing the sensor output. As shown in Fig. 4, for frequencies >1 Hz, we observe an apparent magnetic field change of $\sim 16~\mathrm{pT/mA_{rms}}$ change in heater current with the output response increasing for AM frequencies less than 1 Hz. Together with the observation that the vapor cell thermal time-constant is a few seconds, this supports the supposition that the slow drift in the magnetometer output could be caused by changing cell temperature due to varying heater current. We modeled the magnetic field due to a static current through the heater over the active volume of the vapor cell. The results are shown in the inset of Fig. 4. It is seen that 50 $\mathrm{mA_{rms}}$ current through the heater, generates an average of $\sim 10~\mu T_{rms}$ magnetic field within the cell volume.

Assuming that the atomic precession around the instantaneous magnetic field follows a Lorentzian response function, far from resonance, the atomic response is proportional to $\Gamma^2/\omega^2$, where $\Gamma$ is the Lorentzian line-width and $\omega$ is the excitation frequency. For a typical line-width of $\sim 400$ Hz, corresponding to $\sim 60$ nT magnetic field swing, the atomic response at 30 kHz is suppressed by a factor of about $10^4$. Factoring this in, we find that 1 $\mathrm{mA_{rms}}$ change in the current through the heater at 30 kHz would cause a change in the magnetometer output of 20 pT. This is approximately what is measured experimentally. However, further investigation is required to ascertain the mechanism through which the changing AC magnetic field due to changing heater currents causes a DC offset in the magnetometer output. From a practical standpoint though, this means that the heater current needs to be constant to within 5 $\mu$A for this geometry to achieve a magnetometer sensitivity below 100 $\mathrm{fT_{rms}}/\sqrt{\mathrm{Hz}}$ at 1 Hz. The heater drive frequency can also be increased to mitigate this effect.

## VI. Conclusion

We have described a portable magnetometry system based on a CSAM sensor capable of achieving sensitivities of $\sim 50 \, \mathrm{fT_{rms}}/\sqrt{\mathrm{Hz}}$ at 100 Hz and $\sim 250 \, \mathrm{fT_{rms}}/\sqrt{\mathrm{Hz}}$ at 1 Hz. We find that above 100 Hz the device performance is limited by Johnson noise due to the heaters. At low frequencies, abrupt changes in the heater current cause flicker noise to appear. Preliminary data indicates that the magnetometer stability could be vastly improved if a current source was used to drive the heater instead of a voltage source. This problem can be circumvented by the use of optical means to heat the vapor cell [7]. We believe that CSAM sensors with sensitivities of $10 \, \mathrm{fT_{rms}}/\sqrt{\mathrm{Hz}}$ at 1 Hz based on this approach are certainly feasible. Such a system could be an enabling technology in diverse areas of research from applied neurobiology to fundamental physics.

## Acknowledgment

## References

[1] I.K. Kominis, T.W. Kornack, J.C. Allred and M.V. Romalis, *Nature* **422**, 596 (2003).
[2] S. Knappe, T.H. Sander, O. Kosch, F. Weikhorst, J. Kitching and L. Trahms, *Appl. Phys. Lett.* accepted.
[3] R.L. Fagaly, *Rev. Sci. Instrum.* **77**, 101101 (2006).
[4] K. Sternickel and A.I. Braginski, *Supercond. Sci. Technol.* **19**, S160 (2006).
[5] S. Knappe, V. Gerginov, P.D.D. Schwindt, V. Shah, H.G. Robinson, L. Hollberg and J. Kitching, *Opt. Lett.* **30**, 2351 (2005).
[6] P.D.D. Schwindt, B. Lindseth, S. Knappe, V. Shah, J. Kitching and L.-A. Liew, *Appl. Phys. Lett.* **90**, 081102 (2007).
[7] J. Preusser, V. Gerginov, S. Knappe and J. Kitching, *To be published*.
[8] M.E. Motamedi, "MOEMS: Micro-Opto-Electro-Mechanical systems (SPIE press monograph Vol. PM126)", *SPIE Publications*, (2005).
[9] A.L. Bloom, *Appl. Opt.* **1**, 61 (1962).
[10] H.G. Dehmelt, *Phys. Rev.* **105**, 1924 (1957).
[11] J. Dupont-Roc, S. Haroche and C. Cohen-Tannoudji, *Phys. Rev. A* **28**, 638 (1969).
[12] V. Shah, S. Knappe, P.D.D. Schwindt and J. Kitching, *Nat. Phot.* **1**, 649 (2007).
[13] W. Happer and H. Tang, *Phys. Rev. Lett.* **31**, 273 (1973).
[14] L-A. Liew, S. Knappe, J. Moreland, H. Robinson, L. Hollberg and J. Kitching, *Appl. Phys. Lett.* **84**, 2694 (2004).
[15] C. Cohen-Tannoudji, J. Dupont-Roc, S. Haroche and F. LaLoe, *Rev. Phys. Appl.* **5**, 95 (1970).
[16] S.K. Lee and M.V. Romalis, *J. Appl. Phys.* **103**, 084904 (2008).
[17] R.F. Voss and J. Clarke, *Phys. Rev. B* **13**, 556 (1976).